Hollow cathode glow discharge in He: Monte Carlo–Fluid model combined with a transport model for the metastable atoms

N. Baguer,[a] A. Bogaerts, and R. Gijbels
Department of Chemistry, University of Antwerp (UIA), Universiteitsplein 1, B-2610 Wilrijk-Antwerp, Belgium

(Received 20 February 2002; accepted 10 September 2002)

A hollow cathode discharge (HCD) in He is studied based on a Monte Carlo–fluid hybrid model combined with a transport model for metastable He atoms. The Monte Carlo model describes the movement of fast electrons as particles, while in the fluid model, the slow electrons and positive ions are treated as a continuum. The continuity equations are solved together with the Poisson equation in order to obtain a self-consistent electric field. The He metastable transport model considers various production and loss mechanisms for He metastable atoms. These three models are run iteratively until convergence is reached. Typical results are, among others, the excitation and ionization rates, the electron, ion, and metastable densities and fluxes, the electric field, and potential distribution. The relative importance of different processes determining the metastable density in a He HCD is analyzed, as well as the role of He metastable atoms and He ions on the secondary electron emission at the cathode. Calculation results are compared with experimental data for the same discharge conditions, and good agreement was obtained. © *2003 American Institute of Physics.* [DOI: 10.1063/1.1518784]

I. INTRODUCTION

The cylindrical hollow cathode discharge is a type of glow discharge in which the cathode is wrapped onto itself to form a hollow cylinder, hence the negative glow and cathode fall region are surrounded by cathode surface.[1,2] The anode (or anodes) is placed mostly at the ends of the cathode cylinder and can be chosen in different shapes, such as a disk, a ring, a cylinder, etc. If the distance between the anode and cathode is larger than the cathode region [i.e., cathode dark space (CDS) plus negative glow (NG)] for a given pressure, a positive column can be formed.[3] Due to its special geometric configuration, almost all ions that are created in the NG can hit the cathode surface, contributing to the emission of secondary electrons from the cathode. These electrons, being accelerated in the CDS, can use all their energy for ionization and excitation collisions with the gas atoms and the sputtered cathode material. Moreover, some of these electrons can penetrate into the CDS opposite to the cathode of their origin and cause ionization collisions there, that is, they can oscillate between opposite cathode surfaces (''pendulum effect'').[4–6] As a consequence, the ionization and excitation rates in the CDS and in the NG are enhanced. This enhancement is most evident when the NG regions from facing cathode surfaces overlap, giving rise to a large increase in the current density and light intensity, which is called the ''hollow cathode effect.'' [7–9]

HCDs are being used in a wide variety of application fields, such as plasma processing (ion etching, thin film deposition, surface treatment),[10] lasers[11–13] and spectroscopic analysis.[14–18] To improve the results in these application fields, it is important to understand the different mechanisms involved in the discharge. This can be achieved by numerical modeling. In this work we present a model for He ions and electrons, as well as for metastable He atoms.

The general processes that determine He metastable atom density in a He discharge were first studied by Ebbinghaus.[19] Since then many papers have been published in which the metastables are being studied either experimentally (using atomic absorption spectroscopy,[20,21] plasma induced emission spectroscopy,[22] Doppler shift Fourier transform spectroscopy,[23] etc.), as well as theoretically (the transport of metastable atoms is described by continuity equations, yielding the metastable density).[24,25] The metastable population in He was studied, experimentally and with the use of balance equations, in various kinds of discharges, including afterglow discharges,[26–28] dc,[29] rf[30] and HCDs.[31,32] Studies have also been performed with respect to the role of metastables in a glow discharge with formation of a positive column.[33,34]

In the present article, we analyze the role of the metastables in a HCD, using a metastable transport model, which is combined with a Monte Carlo and a fluid model for electrons and He ions. A similar combination of models has been applied in the literature for the simulation of glow discharges with planar cathode, both for a dc glow discharge in Ar[35] and for an rf discharge in various gases.[25] The advantage of this procedure is that it allows us to follow the influence of the metastable atoms on the electron energy distribution, the ionization rates, the ion and electron densities, etc. and, on the other hand, to explore how these parameters can influence the metastable density. Moreover, as will be shown later, it appeared necessary to include the He metastables in our

[a]Electronic mail: baguer@uia.ua.ac.be

model, in order to account for sufficient ionization in the plasma.

Our calculation results will be compared with experimental data[36] obtained for the same discharge geometry and conditions, as well as with reported data in the literature.

II. DESCRIPTION OF THE NUMERICAL MODEL

A. Assumptions of the model

The discharge gas was assumed to be helium at room temperature and uniformly distributed throughout the discharge. The plasma species considered in the model are: neutral ground state and metastable He atoms, positive ions (He^+), and electrons. The electrons are split up in two groups: the fast electrons, with high enough energies to cause inelastic collisions, and the slow electrons.[37] The two metastables levels of He, the triplet 2^3S and singlet 2^1S metastable levels lying at 19.82 and 20.61 eV above the ground state, respectively, have been combined into one collective level lying at 19.82 eV. This assumption was made because for our purpose only the total metastable density is important. It is found in the literature that the triplet state has a higher density than the singlet state, because the singlet metastables are converted into the triplet metastables by superelastic collisions with slow electrons in the NG; hence, the population of the 2^1S metastable level is typically around 20% of that of the 2^3S metastable level.[25,27,30]

The hybrid model presented here is a combination of three models:

(i) A Monte Carlo model for the fast electrons in the whole discharge,
(ii) a fluid model for the He ions in the entire discharge and for the slow electrons in the NG (indeed the slow electrons are present only in the NG, because in the CDS they always gain energy from the electric field so that they become fast again), and
(iii) a transport model for He metastable atoms.

In the following, these three different models will be described.

B. Monte Carlo model

The Monte Carlo (MC) model simulates the trajectories and collisions of electrons emitted by the cathode as well as the ones created within the discharge gap by ionization.[38–41] The electrons move under the influence of a spatially dependent electric field through a gas of neutral atoms, assumed to be at rest in comparison with the high speed of the electrons. The position at which the secondary electrons are ejected from the cathode walls is determined based on the distribution of the ion and metastable fluxes to the walls [obtained from the fluid and metastable model, respectively (see Sec. II C and II D)]. The electrons are assumed to be emitted in the forward direction with an initial energy of 4 eV.[4] During each time-step, the trajectory of the electrons is calculated with Newton's-laws:

$$X = X_0 + V_{0x}\Delta t - \frac{1}{2m}E_{\mathrm{fr}}\cos\alpha\Delta t^2,$$

$$V_x = V_{0x} - \frac{1}{m}E_{\mathrm{fr}}\cos\alpha\Delta t,$$

$$Y = Y_0 + V_{0y}\Delta t - \frac{1}{2m}E_{\mathrm{fr}}\sin\alpha\Delta t^2,$$

$$V_y = Y_{0y} - \frac{1}{m}E_{\mathrm{fr}}\sin\alpha\Delta t,$$

$$z = Z_0 + V_{0z}\Delta t - \frac{1}{2m}E_{\mathrm{fz}}\Delta t^2, \quad V_z = V_{0z} - \frac{1}{m}E_{\mathrm{fz}}\Delta t,$$

where E_{fz} and E_{fr} are the axial and radial electric field, α is the azimuthal angle of the radial position, m is the electron mass, Δt is the time interval, and X,Y,Z (V_x, V_y, V_z) and X_0, Y_0, Z_0 (V_{0x}, V_{0y}, V_{0z}), are the positions (and velocities) after and before Δt, respectively.

The probability of collision during the time step Δt is calculated by: $P = 1 - \exp\{-\Delta s[n_{\mathrm{He}}\Sigma_j\sigma_j(\epsilon) + n_{\mathrm{He^m}}\sigma_{\mathrm{ion}}(\epsilon)]\}$, where Δs is the distance traveled by an electron with energy ϵ during the interval Δt, n_{He} and n_{He^m} are the density of the He atoms in the ground and metastable state, respectively. $\sigma_j(\epsilon)$ and $\sigma_{\mathrm{ion}}(\epsilon)$ are the electron impact cross sections of the j collisions with He atoms in the ground state (elastic, excitation, and ionization) and of the ionization collision with He atoms in the metastable state, respectively. The cross section for electron impact ionization and excitation from the He ground state and for elastic collision with He ground state atoms are adopted from Phelps,[42] whereas the cross section for electron impact ionization from the He metastable level is taken from Kato *et al.*[43] The calculated collision probability is compared with a random number (r_n), uniformly distributed in the interval between 0 and 1. If $r_n < P$, a collision occurs. To determine the kind of collision a second r_n is generated and compared with the relative probability of each collision. Moreover, electron impact excitation from the He ground state to the He metastable level is explicitly taken into account. That is, if an excitation collision happens, the relative probability of the excitation to the metastable state to the total excitation ($P_{\mathrm{em/et}}$) is calculated and compared with a r_n; if the $r_n < P_{\mathrm{cm/ct}}$, an excitation collision to the metastable level happens. The electron excitation cross section to the metastable level is obtained from Fig. 8 of Ref. 44. After each collision, the new electron energy is calculated depending on the type of the collision. The new direction is determined by anisotropic scattering. The scattering angle χ and the azimuthal angle of scattering ϕ are calculated using two r_n and the differential angular cross section $\sigma(\epsilon, \chi)$ in the same way, as described in Ref. 45. From χ and ϕ the new axial and azimuthal velocity angles are found by transformation of the coordinate frame of reference.[45]

This procedure of following the electrons with Newton's laws and describing their collisions with cross sections and r_n is repeated until the electrons collide at the anodes, where they can be absorbed, reflected, or produce secondary electron emission, or until the electrons are transferred to the

TABLE I. Production and loss processes considered in the model.

Production processes		Rates or rates coefficients
$He+e_f \rightarrow He^m+e_f$	electron-impact excitation	S_{exc} [calculated in MC]
$He^+ +2e \rightarrow He^m+e$	dielectronic recombination	$k_{rec}=6.0\times10^{-20}$ cm^6 s^{-1} [a]
Loss processes		
$He^m+e_f \rightarrow He^+ +2e_f$	electron-impact ionization	S_{ion} [calculated in MC]
$He^m+e \rightarrow He+e+h\nu$	de-excitation	$k_{dexc}=4.2\times10^{-9}$ cm^3 s^{-1} [a]
$He^m+He^m \rightarrow He^+ +He+e_f$	metastable–metastable collision	$k_{met}=1.5\times10^{-9}$ cm^3 s^{-1} [a]
$He^m+He \rightarrow He+He$	two-body collision	$k_{2B}=6.0\times10^{-15}$ cm^3 s^{-1} [b]
$He^m+2He \rightarrow He_2^* +He$	three-body collision	$k_{3B}=2.5\times10^{-34}$ cm^6 s^{-1} [b]
Diffusion to the walls, followed by de-excitation at the walls		$D_{He^m}=470$ cm^2 s^{-1} [b]

[a]Taken from Ref. 28.
[b]Taken from Ref. 27.

slow group, which happens when the sum of their kinetic and potential energy drops below the ionization energy of the combined He metastable level, that is at energies less than 4.77 eV. Indeed, electrons with lower energy are not able to produce inelastic collisions, and can therefore better be described with a fluid model.

C. Fluid model

In the fluid model, the charged particles are considered in hydrodynamic equilibrium with the electric field, and they can be treated as a continuum. They are described with the continuity equations for ions and slow electrons [Eqs. (1) and (2), respectively] and with transport equations (based on diffusion and migration) for ions and slow electrons [Eqs. (3) and (4), respectively]. In order to obtain a self-consistent electric field, these equations are coupled with the Poisson equation [Eq. (5)]. Because of the cylindrical symmetry of the discharge cell (see below), the fluid model is developed in cylindrical coordinates.

Continuity equation for ions;

$$\frac{\partial n_{He^+}}{\partial t}+\nabla\cdot\mathbf{j}_{He^+}=S_{He^+}, \tag{1}$$

Continuity equation for slow electrons;

$$\frac{\partial n_e}{\partial t}+\nabla\cdot\mathbf{j}_e=S_{slow}, \tag{2}$$

Flux equation for ions;

$$\mathbf{j}_{He^+}=-n_{He^+}\mu_{He^+}\nabla V-D_{He^+}\nabla n_{He^+}, \tag{3}$$

Flux equation for slow electrons;

$$\mathbf{j}_c=n_e\mu_e\nabla V-D_e\nabla n_e, \tag{4}$$

Poisson equation;

$$\nabla^2 V=-\frac{e}{\epsilon_0}(n_{He^+}-n_e), \tag{5}$$

where S_{He^+} and S_{slow} are the source terms obtained as output from the Monte Carlo model, representing the number of ions and slow electrons, respectively created per unit volume and per unit time. D_{He^+} and D_c are the ion and slow electron diffusion coefficients, respectively μ_{He^+} and μ_c are the ion and slow electron mobilities, respectively, n_i and n_e are the ion and slow electron densities, respectively, $\mathbf{j}_{He^+}$ and $\mathbf{j}_e$ are the ion and slow electron fluxes, respectively, and V is the electric potential. The values for μ_{He^+} and μ_e were taken from Ward,[46] the value of D_{He^+} was adopted from Deloche *et al.*,[28] and D_e was chosen to be equal to μ_e upon the assumption that the characteristic energy of the slow electrons was constant[47–49] and equal to 1 eV. This value was chosen based on the measurements of the electron energy distribution function in a cylindrical HCD in He, for which the average energy of the electrons was found to be 1.2 eV at 1 Torr.[50] As a consequence of this approximation, some parameters of the discharge that depend directly on the electron temperature, such as the electron density in the NG, will not accurately be calculated, but for the correct description of the CDS, its length, the current voltage characteristic, etc., the most important parameter to be calculated should be the ionization rate, especially by fast electrons, which is calculated in the MC model.[51] On the other hand, with this approximation the model is less complicated, because one does not have to solve the energy equation in the fluid model and one can obtain the energy distribution function for the fast electrons in the MC model.

The previous set of equations is solved with the following boundary conditions:

(i) at the cathode: $V=-$discharge voltage, $n_e=0$, $\nabla n_{He^+}=0$.

(ii) at the anodes: $V=0$, $n_e=0$, $\nabla n_{He^+}=0$.

The system of equations is solved numerically following the procedure developed by Passchier and Goedheer.[52,53]

D. Metastable atom transport model

The behavior of the metastable atoms is also described by a continuity and a transport equation in which the flux is only determined by diffusion.[27,28,35] The different production and loss processes considered in the model are summarized in Table I.

Electron impact excitation of the metastables to higher radiating states is not included as a loss channel because of radiation trapping, that is, most of the electrons excited from the metastables to the radiating states come back to the metastable level due to reabsorption of the emitted light from transition to the ground state.[28,30,33] Taking into account the

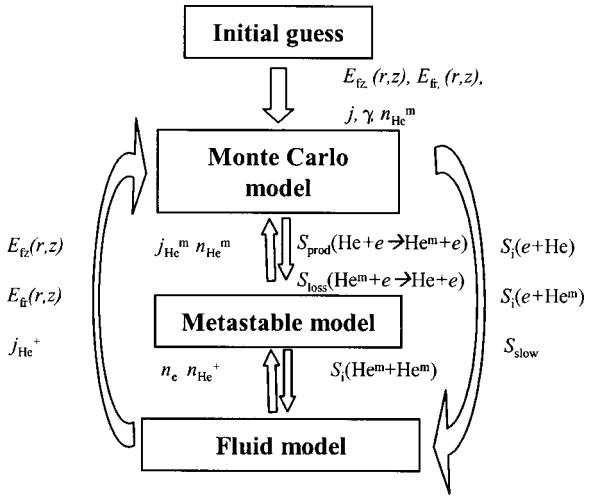

FIG. 1. Flowchart of the hybrid model.

production and loss processes summarized in Table I, the He metastable atoms are described with the following continuity equation:

$$\frac{\partial n_{\mathrm{He^m}}}{\partial t} - D_{\mathrm{He^m}} \nabla^2 n_{\mathrm{He^m}} = S_{\mathrm{prod}} - S_{\mathrm{loss}}, \tag{6}$$

where

$$S_{\mathrm{prod}} = S_{\mathrm{exc}} + k_{\mathrm{rec}} [n_e]^2 n_{\mathrm{He^+}},$$

$$S_{\mathrm{prod}} = S_{\mathrm{ion}} + k_{\mathrm{dexo}} n_{\mathrm{He^m}} n_e + 2k_{\mathrm{met}} [n_{\mathrm{He^m}}]^2 + k_{2\mathrm{B}} n_{\mathrm{He^m}} n_{\mathrm{He}} + k_{3\mathrm{B}} n_{\mathrm{He^m}} [n_{\mathrm{He}}]^2.$$

Equation (6) is discretized and solved with the Thomas algorithm,[54] assuming as boundary condition $n_{\mathrm{He^m}} = 0$ (the same at anodes and cathode).

E. Coupling of the models

The coupling of the models is illustrated in Fig. 1 and is explained as follows:

First, the MC model is run, assuming a linearly decreasing electric field in the CDS and a zero electric field in the NG, uniform ion and metastable fluxes to the cathode walls, and a secondary electron emission coefficient (γ), equal to 0.3,[55,56] which was used only for the first iteration. (For the further iterations it was calculated in each fluid cycle of the model, see below). In this work the γ coefficient could not be calculated directly in the MC model as it was done in Ref. [45], because here, together with the He ions, the metastable He atoms also play an important role in the electron emission from the cathode surface. Output of the MC model used as input in the fluid model includes the ion production rate due to the electron impact ionization (from the ground and metastable states) and the slow electron creation rate. The output of the MC model used for the metastable model is the production rate of the metastable atoms due to electron impact excitation from the ground state, as well as the loss rate of the metastables due to electron impact ionization.

Second, the He metastable model is run with production and loss rates from the MC model. The output of this model includes the ion production rate due to metastable–metastable collisions, which is used in the fluid model, as well as the density of the metastable level and the flux of metastable atoms bombarding the cathode, which are both used in the MC model (to determine the electron impact ionization rate from the metastable level and the secondary electron emission at the cathode due to metastables, respectively).

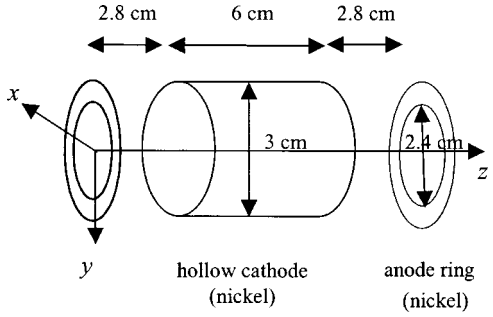

FIG. 2. Schematic picture of the cell geometry assumed in the model.

Next, the fluid model is run with the above source terms, both from the MC and the metastable model. This yields the ion and electron densities and fluxes, the electric field, the ion flux toward the cathode, and γ. The γ coefficient is calculated based on the condition for the current balance at the cathode surface,[3] $\gamma = I^D/I^+ - 1$, where I^D is the total discharge current and the I^+ is the ion current to the cathode surface. The electric field, the ions flux to the cathode, and γ will be used as input for the MC model. The ion and electron densities are used in the metastable model to calculate certain production and loss rates, which are not provided from the MC model.

The above three models are run iteratively until convergence is reached. The latter is determined by the difference in the total current to the anode in two successive iterations, which should be below 1%. Typically, 7 to 10 iterations were carried out before convergence was reached. The total current to the cathode was not taken as a criterion of convergence, because the difference between two successive iterations was already below 1% after a few iterations.

III. RESULTS AND DISCUSSION

A. Geometry and discharge conditions

The calculated results are illustrated here for the same geometry and discharge conditions as used in the experiments reported in Ref. 36, in order to allow the best comparison between calculated and measured data.

The electrodes of the discharge are schematically illustrated in Fig. 2. The hollow cathode is a nickel cylinder with 6 cm length and 3 cm inner diameter, open at both ends. The anodes are rings, with 2.4 cm inner diameter, also made of nickel and located at both ends of the cathode at a distance of 2.8 cm. The discharge conditions assumed in the model are also taken from the experiments, i.e., the gas pressure is 1 Torr, the discharge current ranges from 2 to 6 mA and a discharge voltage between 158 and 170 V is applied to the cathode, whereas the anodes are grounded.

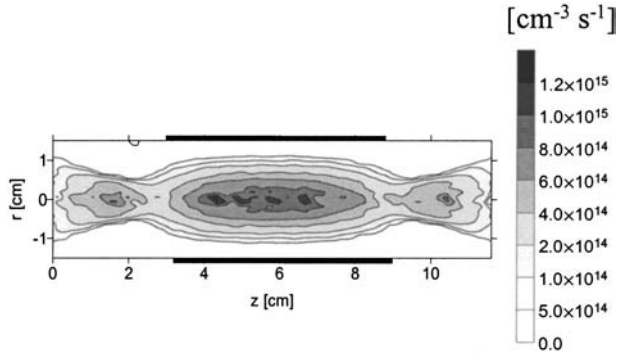

FIG. 3. Calculated two-dimensional electron impact excitation rate to the He metastable level throughout the discharge at a pressure of 1 Torr and a current of 4.5 mA. The hollow cathode is represented by the thick black lines from $z=2.8$ cm to $z=8.8$ cm, whereas the anode rings are located at $z=0$ cm and $z=11.6$ cm.

B. Collision rates

The calculated electron impact excitation rate to the metastable level is presented in Fig. 3, at a current of 4.5 mA, a voltage of 165 V, and a pressure of 1 Torr. Figure 4 shows the calculated total ionization rate (a), as well as the contributions by electron impact ionization from He ground state atoms (b) and from the He metastable level (c), and by ionization due to the metastable–metastable collisions (d), under the same conditions as in Fig. 3. The thick black lines from $z=2.8$ cm to $z=8.8$ cm represent the hollow cathode, whereas the anode rings are located at $z=0$ cm and $z=11.6$ cm (i.e., the borders of the figure).

It appears from these figures that the maximum of all excitation and ionization rates occurs in the NG, more specifically at the discharge center (both in axial and radial direction). Moreover, a second maximum is also observed at the cylinder axis, but in the region between cathode and anode (here termed as anode region) for the electron impact excitation rate to the metastable level (see Fig. 3) and for the ionization rate due to metastable–metastable collisions [see Fig. 4(d)]. Especially for the electron impact excitation rate to the metastable level, the maximum in the anode region is nearly equal to the maximum at the discharge center, as follows from Fig. 3. Keeping in mind that this process is the main source for the production of metastables (indeed, electron–ion recombination is found to be negligible at pressures below 4 Torr),[28,32] it will yield a metastable density in the anode region comparable in magnitude to the metastable density at the discharge center (see Sec. II C). Hence, this will give the profile with a second maximum in the anode region for the metastable–metastable collision rate, as is shown in Fig. 4(d).

As far as the total ionization rate in the discharge is concerned, it appears to reach a maximum only in the cathode region (the discharge cavity inside the cathode cylinder, from $z=2.8$ to 8.8 cm) [see Fig. 4(a)]. The reason is that electron impact ionization from the He ground state is the dominant ionization mechanism in the discharge [see Fig. 4(b)]. The latter ionization mechanism is not only important in the NG, but also in the CDS, where 44% of the electron impact ionization takes place, according to our model calcu-

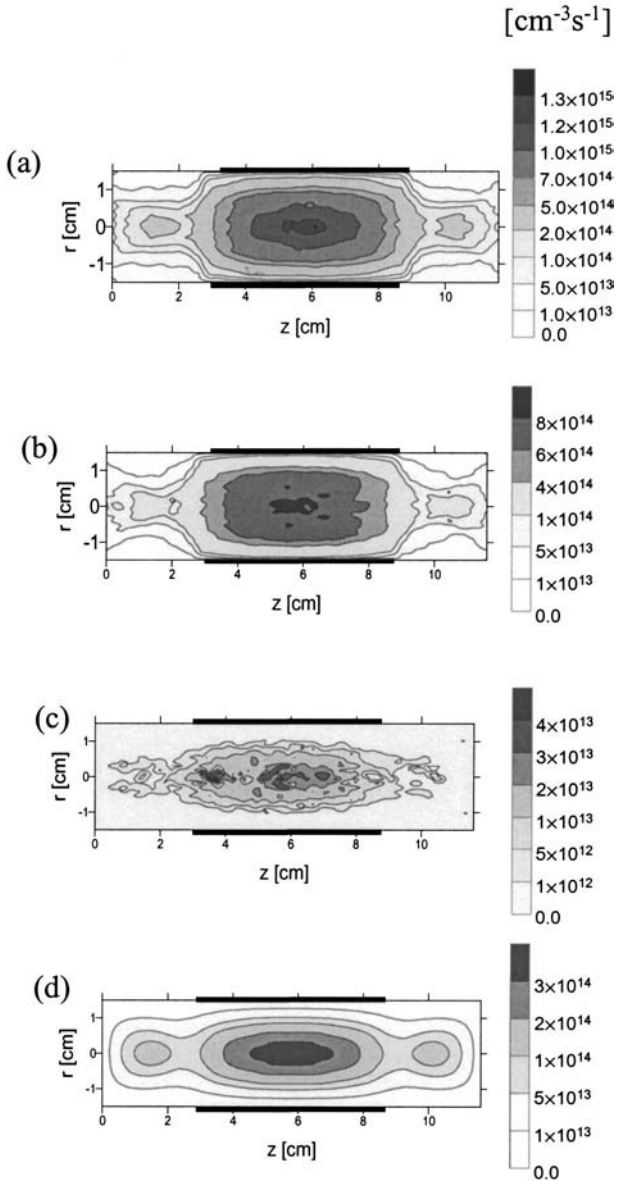

FIG. 4. Calculated two-dimensional ionization rates throughout the discharge at a pressure of 1 Torr and a current of 4.5 mA: (a) total ionization rate, (b) electron impact ionization rate of He ground state atoms, (c) electron impact ionization rate of He metastable atoms, and (d) ionization rate due to metastable–metastable collisions.

lations. The importance of electron impact ionization in the CDS of a HCD at pressures around 1 Torr was also observed in our previous work.[45] Compared to electron impact ionization from the He ground state, ionization due to metastable–metastable collisions [Fig. 4(d)] is the second in importance, but it is more confined to the cylinder axis. Electron impact ionization from the He metastable level, on the other hand, is clearly of minor importance at the conditions under study. Integrated over the total discharge volume, the relative contributions of electron impact ionization from the ground state, ionization due to metastable–metastable collisions, and electron impact ionization from the He metastable level, were calculated to be 81%, 18%, and 1%, respectively, at the conditions under study (see above). With decreasing current, the role of electron impact ionization from the He ground

state becomes even more dominant; for example, at 2 mA, the relative contribution was calculated to be almost 86%. Electron impact ionization from the He metastable level, on the other hand, becomes then almost negligible (calculated to be 0.2% at 2 mA).

Figure 5(a) illustrates the calculated electron impact excitation rates to the He metastable level at $z=5.8$ cm (at the discharge center in the axial direction), as a function of radial position, at three different currents. As expected, the excitation rate increases with rising current. The shape of the curves is quite similar, with a maximum at the cylinder axis. This means that for the three conditions investigated, the NG regions of the two opposite cathode walls overlap, that is the HC effect is present. The shapes of the three curves are compared in more detail in Fig. 5(b), which shows the normalized excitation rates. It appears that the excitation rate is more peaked at the discharge center at the lowest current investigated. In other words, the CDS is somewhat larger at the lowest current, as is expected.[3,57] In Fig. 5(c) the normalized light intensity distributions are plotted as a function of radial position (again at $z=5.8$ cm), at the three different currents, for the line $\lambda=501.6$ nm, corresponding to the transition from $3\ ^1P$ to $2\ ^1S$, as measured in Ref. 36. Exact comparison between Figs. 5(b) and 5(c) is not possible, because our calculation results show the excitation rate to the He metastable level, whereas the experimental light intensity originates from another excited level. However, the latter still reflects the electron impact excitation rate.[45,58,59] It is clear that the same behavior is observed in both calculated and measured results. Indeed, Fig. 5(c) shows that the light intensity distribution is also somewhat more peaked at the cylinder axis, that is the CDS extends to slightly further distances from the cathode walls, at the lowest current of 2 mA, which is in accordance with our calculation results.

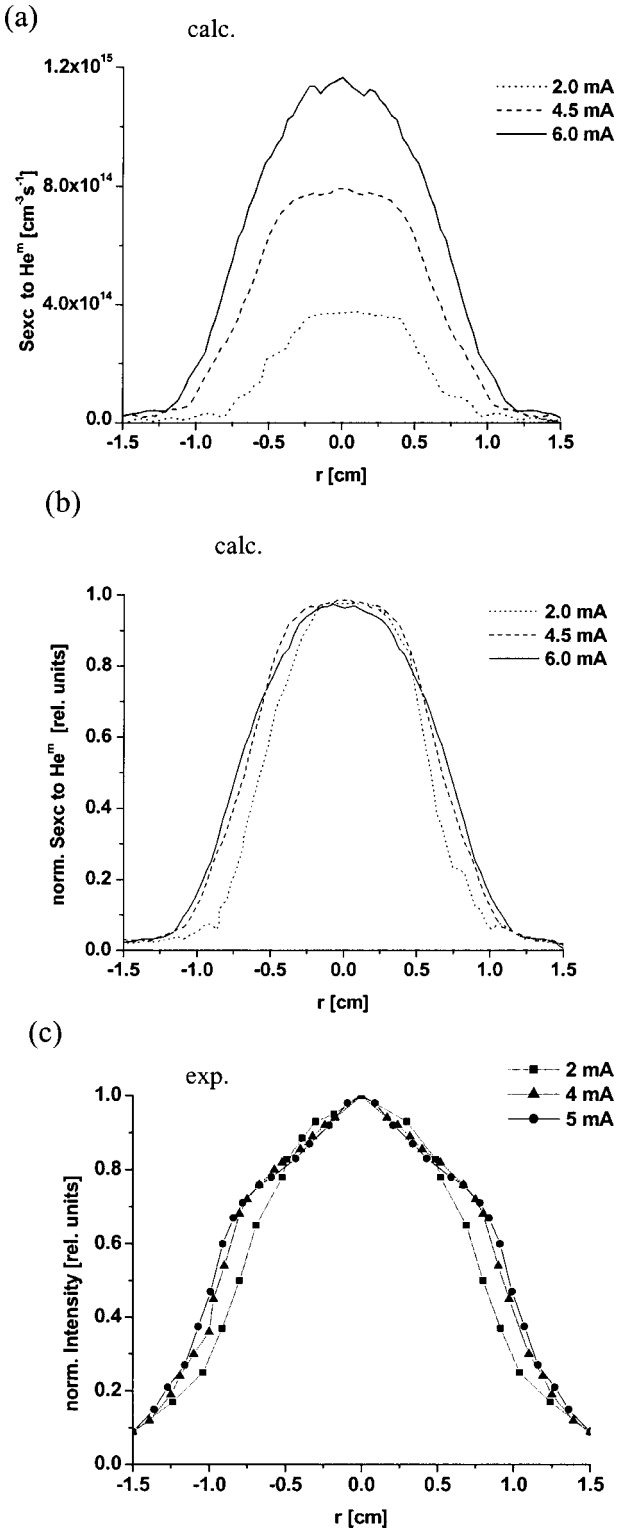

FIG. 5. Radial profiles at $z=5.8$ cm for 1 Torr and three different currents: (a) calculated electron impact excitation rates to the He metastable level, (b) normalized calculated electron impact excitation rates to the He metastable level, and (c) normalized measured light intensity distribution for the HeI line at 501.6 nm.[36]

C. Electron, ion, and metastable densities

Figure 6 presents the calculated two-dimensional density profiles of (a) electrons, (b) He ions, and (c) He metastable atoms at a current of 4.5 mA. Whereas the electron and He ion densities reach a maximum only within the HC region, the He metastable density is characterized by a second maximum outside the HC region, that is, in the so-called anode region, as was predicted by the shape of the electron impact excitation rate (see Sec. III B). When comparing the absolute values of the densities, it appears that the He metastable atom density is about one order of magnitude higher than the He ion and electron densities, at the current of 4.5 mA. The metastable density changes only slightly with variation of the current, that is the maximum value varies from 1.6×10^{11} cm^{-3} at 2 mA, over 2.8×10^{11} cm^{-3} at 4.5 mA, to 3.8×10^{11} cm^{-3} at 6 mA. The electron and He ion densities, on the other hand, are more dependent on current (see below). Therefore, the ratio of He metastable to He ion or electron densities is higher at lower current. For example, at 2 mA, the He metastable atom density at the discharge center was calculated to be 30 times higher than the electron and He ion densities, whereas it was only 7 times higher at 6 mA.

Figure 7 illustrates the calculated electron densities at $z=5.8$ cm, as a function of radial position, at the three currents under study (a), in comparison to the measured data (b), from Ref. 36. The calculated electron densities appear to be somewhat higher, and they rise more uniformly with in-

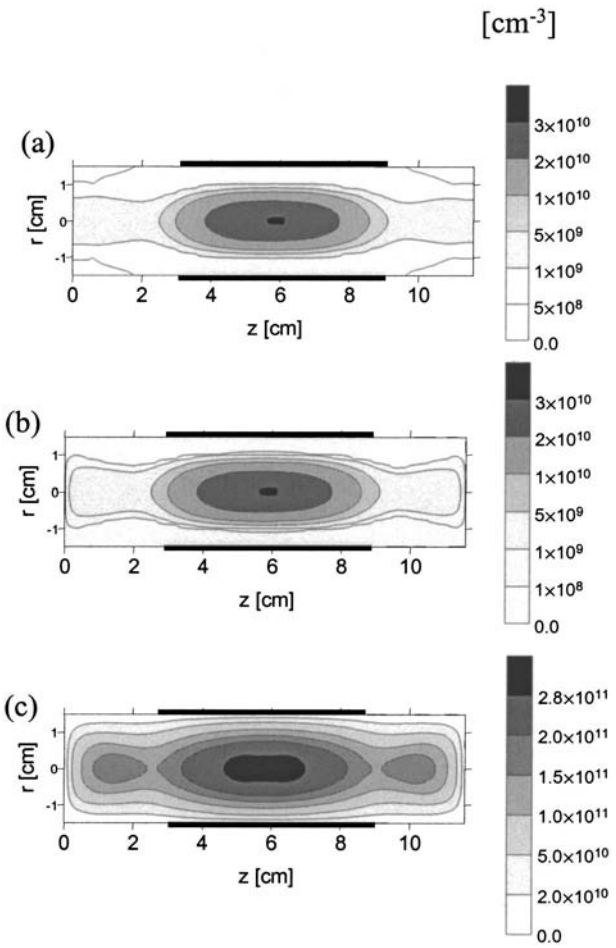

FIG. 6. Calculated two-dimensional density profiles throughout the discharge at a pressure of 1 Torr and a current of 4.5 mA, for the (a) slow electrons, (b) the ions, and (c) the He metastable atoms.

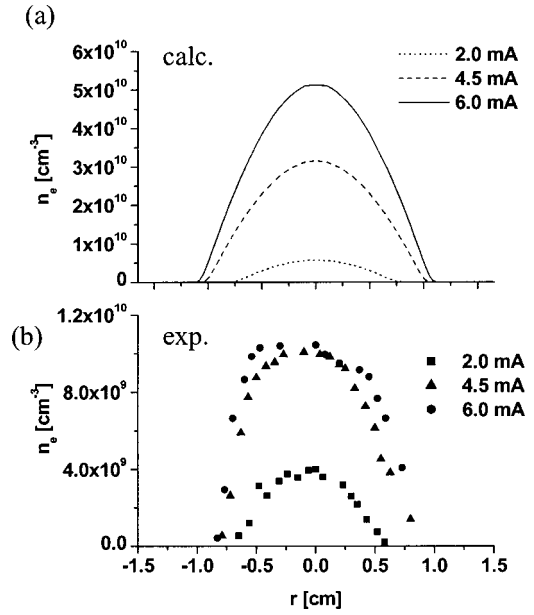

FIG. 7. Radial dependence of the slow electron density at $z=5.8$ cm for a pressure of 1 Torr and three different currents: (a) calculated results and (b) experimental data obtained from Ref. 36.

creasing current, in comparison with the experimental data (where the difference between 4.5 and 6 mA was found to be very small). This difference between the calculated and experimental value of the electron density may be a direct consequence of the assumption of constant electron temperature in the simulations. Nevertheless, keeping in mind that both calculations and measurements are subject to uncertainties, the agreement is already quite satisfactory, because both calculated and measured densities are in the same order of magnitude, and show the same radial dependence.

Concerning the importance of the different processes determining the metastable density, it was found for the conditions under study that the production occurs almost completely by electron impact excitation, and that electron–ion recombination is negligible. Indeed, as reported from measurements in Ref. 32, recombination becomes only important for the production of He metastable at pressures above 4 Torr. As far as the loss of metastables is concerned, diffusion and subsequent de-excitation at the walls is most significant (the relative contribution, integrated over the entire discharge region, is calculated to be 60% at 4.5 mA), followed by metastable–metastable collisions (28%) and two-body collisions with He ground state atoms (8%). The other loss processes considered in the model are found to be negligible at the conditions under study. At decreasing current, the role of diffusion becomes even more important, with a calculated contribution of 76% at 2 mA.

Because of the high He metastable atom density compared to the He ion and electron densities, it is expected that the flux of metastable atoms to the cathode walls play an important role in secondary electron emission.[27] Indeed, the metastable atom flux to the cathode walls is about 15% of the total flux (ion plus metastable) at 6 mA, and this value increases with decreasing current, 17% at 4.5 mA, and 20% at 2 mA. If we consider that the electron emission yield due to the He metastables is comparable in magnitude to the He ion induced emission yield, as was measured by Hasted,[60] the role of He metastables in secondary electron emission reflects the contribution to the total flux, and hence is not negligible. As appears from above, it increases slightly with decreasing current. The same tendency was observed for the γ coefficient: at $I=6$, 4.5, and 2 mA, γ was equal to 0.32, 0.38 and 0.44, respectively. As was said earlier the γ coefficient calculated in this work reflects the total contribution of the ions and metastable atoms in the emission of secondary electrons from the cathode surface. Indeed, in the fluid model, where it was calculated, the source terms of the continuity equations include the collision rates due to the fast electron impact ionization with He atoms in ground and metastable states (calculated in the MC cycle of the model), and the ionization due to collisions between pairs of metastable He atoms (calculated in the metastable cycle of the model). We can then guess that the γ increment at low currents is related to the increased efficiency of the metastable atoms in releasing electrons from the cathode surface; this can compensate to some degree for the drop in the relative contribution to ionization (i.e., electron multiplication in the discharge) by metastable–metastable collisions at lower currents (see Sec. III B).

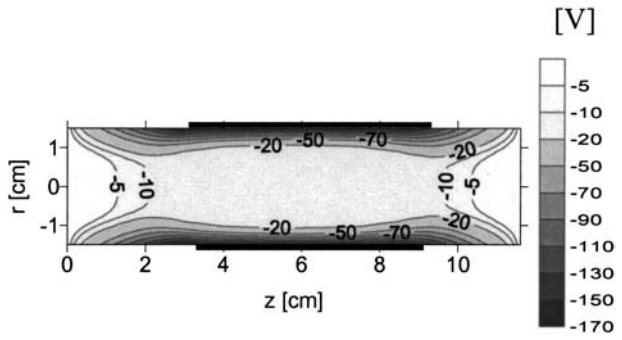

FIG. 8. Calculated two-dimensional potential distribution throughout the discharge at a pressure of 1 Torr and a current of 4.5 mA.

In general, it can be concluded that the role of He metastables in the production of electrons and ions (and hence electrical current), both with respect to secondary electron emission and to ionization in the plasma, is not negligible in the He HCD for the conditions under study. In fact, we found that it was necessary to include the He metastable atoms in our model, in order to account for sufficient electron and ion production, and hence to calculate an electrical current in correspondence to the experimental values.

D. Potential and electric field distribution

The two-dimensional electric potential distribution throughout the discharge is depicted in Fig. 8. The two characteristic regions in the HCD, the CDS and NG, can be clearly distinguished. It is interesting to notice that the equipotential lines in the CDS are concave within the HC region, whereas they are convex outside this region. In this way, they will focus the electrons inside the HC region toward the discharge center, and outside this region toward the center of the anode rings. It is clear that the potential in the CDS changes rapidly from -165 V at the cathode walls to about -20 V at about 5 mm from the cathode, that is, at the CDS–NG interface. In the NG, no field reversal is observed, the plasma potential remains negative and it is rather constant (varying from -20 V at the CDS–NG interface to -11 V at the discharge center). Indeed, there is no need for the plasma potential to become positive in order to guarantee the discharge current balance,[45] as is the case in other kinds of glow discharges. In Ref. 61 it is argued that the field reversal appears in order to decrease the loss of fast electrons to the anode, and in Ref. 62 it was mentioned that if almost all positive ions flow to the cathode, and if this is compensated by a flux of electrons to the anode, no field reversal is necessary. Both conditions are fulfilled in a cylindrical HCD, that is due to its geometry, the positive ions in the NG will diffuse radially to the NG–CDS interface, while the slow electrons, which are trapped radially, will flow in the axial direction to the anodes (only the slow electrons are trapped). The radial current (to the cathode) will be carried mainly by the ions, while the axial current (to the anodes) will be due mainly to the slow electrons, that is, the ion and electron fluxes occur preferentially in different directions. The loss of fast electrons to the anode is reduced, because the fast electrons can oscillate between the opposite CDS (pendulum effect), releasing their energy inside the cathode cavity by inelastic collisions.

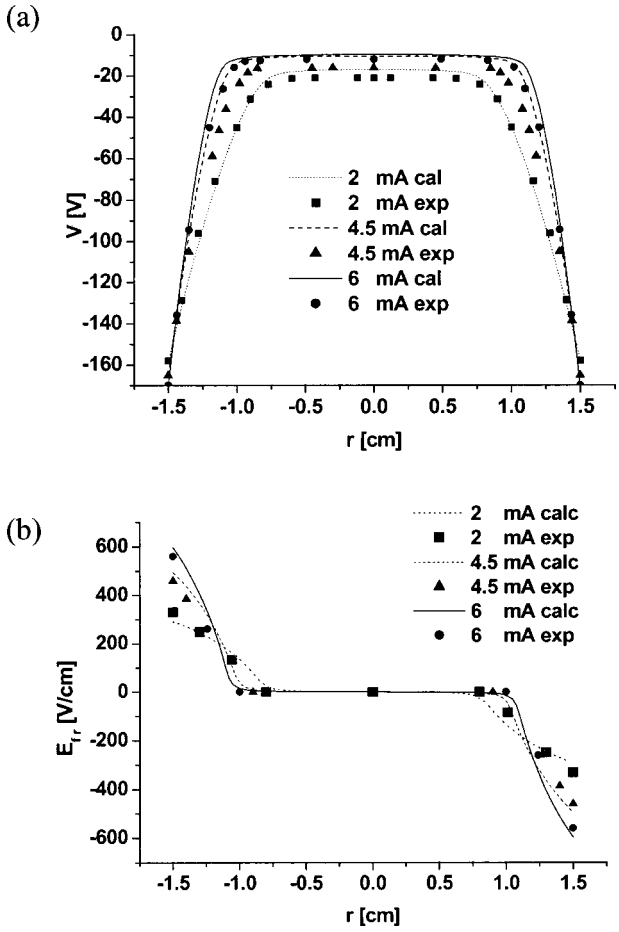

FIG. 9. Radial profiles of the (a) calculated electric potential and (b) radial electric field distribution, at $z=5.8$ cm for a pressure of 1 Torr at three different currents, (curves), compared with experimental data obtained from Refs. 36 and 63 (symbols).

Figure 9 shows the calculated radial profiles, at $z=5.8$ cm, of the (a) electric potential and (b) radial electric field, at the three different currents under study. Also illustrated in these figures are the corresponding measured values, as obtained from Refs. 36 and 63. Very good agreement is reached between calculated and measured data, both with respect to the length of the CDS (cf. the change in gradient in potential and electric field distribution) and to the value of the plasma potential in the NG. The latter is found to be negative and of similar magnitude in both calculated and measured results. Moreover, it becomes slightly more negative with decreasing current.

IV. CONCLUSIONS

A hybrid model, consisting of a MC model for the fast electrons, a fluid model for the slow electrons and He ions, and a transport model for the He metastable atoms, has been developed for a He HCD. Typical calculation results, such as the excitation and ionization rates, the plasma species densities, and the potential and electric field distribution, are illus-

trated, and compared with available experimental data[36,63] for the same cell geometry and discharge conditions, to check the validity of the calculations.

It was found that the excitation and ionization rates, as well as the plasma species densities, reach a maximum at the discharge center, both in axial direction (in the middle of the HC region, at $z=5.8$ cm) and in radial direction (at the cylinder axis). The He metastable atoms also reach, however, a second maximum outside the HC region, that is, in the region between HC and anode rings. The reason is that the dominant production mechanism of the He metastables, electron impact excitation to the metastable level, also reaches a second maximum in this region.

The calculated He metastable atom density was found to be an order of magnitude higher than the calculated electron and He ion densities at the intermediate current of 4.5 mA. Consequently, the role of He metastable atoms is clearly not negligible at the conditions under study, both with respect to secondary electron emission at the cathode walls, and to ionization in the plasma, by metastable–metastable collisions. The latter process typically accounts for about 20% to the total ionization in the HCD, according to our model calculations. Therefore, it was found that including the He metastables in the model was necessary to be able to reproduce the experimental electrical current values.

Finally, the comparison made with the experimental data of Refs. 36 and 63, for the electrical current, and the radial profiles of electron density, potential, and radial electric field (including the value of the plasma potential and the CDS length), shows that the model presents a realistic picture of the He HCD.

ACKNOWLEDGMENTS

One of the authors (N. B.) is financially supported by a New Research Initiative of the University of Antwerp. One author (A. B.) is indebted to the Flemish Fund for Scientific Research (FWO) for financial support. This research is also sponsored by the FWO research project G.0043.01, by NATO's Scientific Affairs Division in the framework of the Science for Peace Programme, and by the Federal Services for Scientific, Cultural and Technical Affairs of the Prime Minister's Office through IUAP V. Finally, we would like to thank M. Otte and his colleagues from the University of Greifswald for providing us the experimental data and for interesting discussions.

[1] F. Paschen, Ann. Phys. (Leipzig) **50**, 901 (1916).
[2] F. Paschen, Ann. Phys. (Leipzig) **71**, 537 (1923).
[3] A. von Engel, *Ionized Gases* (Claredon, Oxford, 1965).
[4] H. Helm, Naturforscher **27a**, 1812 (1972).
[5] A. Guntherschulze, Z. Phys. **2**, 49 (1930).
[6] G. Stockhausen and M. Kock, J. Phys. D **34**, 1683 (2001).
[7] P. F. Little and A. von Engel, Proc. R. Soc. London **224**, 209 (1954).
[8] V. I. Kolobov and L. D. Tsendin, Plasma Sources Sci. Technol. **4**, 551 (1995).
[9] R. R. Arslanbekov, A. A. Kudryavtsev, and R. C. Tobin, Plasma Sources Sci. Technol. **7**, 310 (1998).
[10] A. Goldamn and J. Amoroux, *Gases: Macroscopic Processes and Discharges* (Plenum, New York, 1983).
[11] K. Rozsa, Z. Naturforsch. A **35A**, 649 (1980).
[12] I. G. Ivanov, E. L. Latush, and M. F. Sem, *Metal Vapors Ion Lasers: Kinetic Processes and Gas Discharges* (Wiley, Chichester, 1996).
[13] N. K. Vuchkov, K. A. Temelkov, and N. V. Sabotinov, IEEE J. Quantum Electron. **35**, 1799 (1999).
[14] E. M. Oks, A. V. Vizir, and G. Y. Yushkov, Rev. Sci. Instrum. **69**, 853 (1998).
[15] P. J. Slevin and W. W. Harrison, Appl. Spectrosc. Rev. **10**, 201 (1975).
[16] S. Caroli, Prog. Anal. At. Spectrosc. **6**, 253 (1983).
[17] K. Gilmodinov, B. Radziuk, M. Sperling, B. Welz, and K. Nagulin, Appl. Spectrosc. **49**, 413 (1995).
[18] C. Schepers, J. A. C. Broekaert, J. Anal. At. Spectrom. **15**, 61 (2000).
[19] E. Ebbinghaus, Ann. Phys. (Leipzig) **7**, 267 (1930).
[20] A. McIntonsh, M. H. Dunn, and I. K. Belai, J. Phys. D **11**, 301 (1978).
[21] K. E. Greenberg and G. A. Hebner, J. Appl. Phys. **73**, 8126 (1993).
[22] T. Kubota, Y. Morisaki, A. Ohsawa, and M. Ohuchi, J. Phys. D **25**, 613 (1992).
[23] H. S. Myeong, H. Xichun, and T. A. Miller, Chem. Phys. **228**, 145 (1998).
[24] T. Ledig and B. Schroder, J. Phys. D **25**, 1080 (1992).
[25] T. J. Sommerer and M. Kushner, J. Appl. Phys. **71**, 1654 (1992).
[26] A. V. Phelps, Phys. Rev. **89**, 1202 (1952).
[27] A. V. Phelps, Phys. Rev. **99**, 1307 (1955).
[28] R. Deloche, P. Monchicourt, M. Cheret, and F. Lambert, Phys. Rev. A **13**, 1140 (1976).
[29] E. A. Den Hartog, T. R. O'Brian, and J. E. Lawler, Phys. Rev. Lett. **62**, 1500 (1989).
[30] H. M. Katsch, E. Quandt, and Th. Schneider, Plasma Phys. Controlled Fusion **38**, 183 (1996).
[31] P. Gill and C. E. Webb, J. Phys. D **10**, 299 (1977).
[32] I. Kuen, F. Howorka, and H. Stori, Phys. Rev. A **23**, 829 (1981).
[33] P. G. Browne and M. D. Dunn, J. Phys. B **6**, 1103 (1973).
[34] K. A. Hardy and J. W. Sheldon, J. Appl. Phys. **53**, 8532 (1982).
[35] A. Bogaerts and R. Gijbels, Phys. Rev. A **52**, 3743 (1995).
[36] S. Pfau, R. Kosakov, M. Otte, and J. Rohmann, in Proceedings of the XXIV ICPIG, Warsaw, 1999, p. 33.
[37] M. Surendra, D. B. Graves, and G. M. Jellum, Phys. Rev. A **41**, 1112 (1990).
[38] A. Tran Ngoc, E. Marode, and P. C. Johnson, J. Phys. D **10**, 2317 (1977).
[39] J. P. Boeuf and E. Marode, J. Phys. D **15**, 2169 (1982).
[40] S. Hashigushi and M. Hasikuni, Jpn. J. Appl. Phys., Part 1 **21**, 1010 (1988).
[41] A. Bogaerts, M. van Straaten, and R. Gijbels, Spectrochim. Acta, Part B **50**, 179 (1995).
[42] A. V. Phelps (private communication); ftp://jila.colorado.edu/collision_data
[43] T. Kato and R. K. Janev, Atomic and Plasma-Material Interaction Data for Fusion (suppl. to Nucl. Fusion) **3**, 33 (1992).
[44] L. L. Alves and C. M. Ferreira, J. Phys. D **24**, 591 (1991).
[45] N. Baguer, A. Bogaerts, and R. Gijbels, Spectrochim. Acta, Part B **57**, 311 (2002).
[46] A. L. Ward, J. Appl. Phys. **33**, 2789 (1962).
[47] A. Fiala, L. C. Pitchford, and J. P. Boeuf, Phys. Rev. E **49**, 5607 (1994).
[48] Z. Donko, Phys. Rev. E **57**, 7126 (1998).
[49] K. Kutasi and Z. Donko, J. Phys. D **33**, 1081 (2000).
[50] M. A. Khodororovskii, Ph. D. thesis, University of St. Petersburg, 1975.
[51] P. Boeuf and L. C. Pitchford, J. Phys. D **28**, 2083 (1995).
[52] D. Paschier, Ph. D. thesis, University of Utrecht, 1994.
[53] D. Paschier and W. J. Goedheer, J. Appl. Phys. **74**, 3744 (1993).
[54] D. U. Rosenberg, *Methods for the Numerical Solutions of Partial Differential Equations* (Elsevier, New York, 1969).
[55] F. Stebbings, Proc. R. Soc. London, Ser. A **241**, 270 (1957).
[56] E. A. Den Hartog, D. A. Doughty, and J. E. Lawler, Phys. Rev. A **38**, 2471 (1988).
[57] F. Howorka and M. Pahl, Naturforscher **27a**, 1425 (1972).
[58] A. Bogaerts, R. Gijbels, and J. Vleck, Spectrochim. Acta, Part B **53**, 1517 (1998).
[59] T. Kubota, Y. Morisaki, A. Ohsawa, and M. Ohuchi, J. Phys. D **25**, 613 (1992).
[60] J. B. Hasted, J. Appl. Phys. **30**, 22 (1959).
[61] T. J. Sommerer, W. N. G. Hitchon, and J. E. Lawler, Phys. Rev. A **39**, 6356 (1989).
[62] R. A. Gottsho, A. Mitchell, R. Scheller, Y. Y. Chan, and D. B. Graves, Phys. Rev. A **40**, 6407 (1989).
[63] M. Otte (private communication).